Bifurcation of drift shells near the dayside magnetopause

M. Kaan Öztürk[1,2] and R. A. Wolf[1]

Received 26 September 2006; revised 20 February 2007; accepted 1 March 2007; published 10 July 2007.

[1] Close to the dayside magnetopause, there is a region of space where each field line has two magnetic field minima, one near each cusp. That region is located around local noon, and extends about $1-2\ R_e$ from the magnetopause. Particles that enter this region with equatorial pitch angles sufficiently close to 90° will cross the dayside not along an equatorial path, but along one of the two branches on either side of the equatorial plane. The two branches are joined again past local noon. This process of drift-shell bifurcation (DSB) is nonadiabatic even under static conditions. Two physical mechanisms can cause this nonadiabaticity: one that is operative for nearly all magnetospheric magnetic field configurations and another that depends on a particular combination of north-south and east-west asymmetry in the magnetic field. This paper deals only with the first mechanism. For configurations with north-south and east-west symmetry, DSB changes the second invariant I of the motion by a small amount that is of the order of the gyroradius (the first invariant is intact). For near-equatorial particles ($I \approx 0$) the change can be significantly larger. Assuming north-south and dawn-dusk symmetry, we present general theoretical expressions for the second-invariant jump ΔI, which can be applied to a variety of magnetic field models. The results show that ΔI is sensitively dependent on the bounce phase of the particle at the bifurcation line. The RMS value of ΔI over a bounce-phase ensemble increases with decreasing mirror field and with increasing kinetic energy. We verify these results with test-particle simulations using model magnetic fields.

Citation: Öztürk, M. K., and R. A. Wolf (2007), Bifurcation of drift shells near the dayside magnetopause, *J. Geophys. Res.*, *112*, A07207, doi:10.1029/2006JA012102.

1. Introduction

[2] The familiar picture of a toroidal drift-shell, though accurate near the Earth where the field does not significantly deviate from dipolar, breaks down in a region near the magnetopause, where the compression by the solar wind provides a significant perturbation. Let $B(s)$ be the field strength along a given field line parameterized by s: over field lines that cross the Earth's surface at low-to-intermediate latitudes (low L), $B(s)$ has a single minimum, located near the magnetic equator. On the other hand, field lines with high L values come sufficiently close to the dayside magnetopause so that they are influenced by the external field. Because of this influence, the field profile $B(s)$ for such a field line has one local maximum at the equator, and two local minima near the cusps. Therefore along high-L lines $B(s)$ is W-shaped, whereas along dipole-like (low-L) field lines it is U-shaped.

[3] In this paper, we limit our theoretical treatment to magnetic field models that have symmetry about the $z = 0$ plane. As discussed briefly in section 7, another DSB-associated mechanism may operate for magnetic field configurations that lack symmetry about both the $z = 0$ and $y = 0$ planes. That mechanism will be the subject of a follow-up paper.

[4] Figure 1 shows a generic picture of the relevant region in the equatorial plane. For reasons that will become clear in following paragraphs, this region of space where the field lines have a W-shaped field profile is called "the bifurcation region". The figure assumes that the field is symmetric with respect to the equator. The second derivative of the field strength along the field line, $\frac{d^2B}{ds^2}$, is negative in the bifurcation region, indicating a local maximum, and positive everywhere else.

[5] The differences among field lines in terms of strength profile have significance for particle motion because the function $B(s)$ (multiplied by the first invariant μ) acts as a potential energy for the bounce motion along the field line. Therefore if a test particle is initialized on a field line with W-shaped $B(s)$, such that its mirror field B_m is less than the local maximum value of $B(s)$, the bounce motion will not be able to cross the equator and will be confined to the neighborhood of one of the side minima. The existence of a local maximum along field lines as described here, and its implications for bounce motion, is discussed in early studies such as the works of *Mead* [1964], *Northrop and Teller*

[1]Department of Physics and Astronomy, Rice University, Houston Texas, USA.
[2]Now at the Department of Information Technologies, Işık University, İstanbul, Turkey.

0148-0227/07/2006JA012102

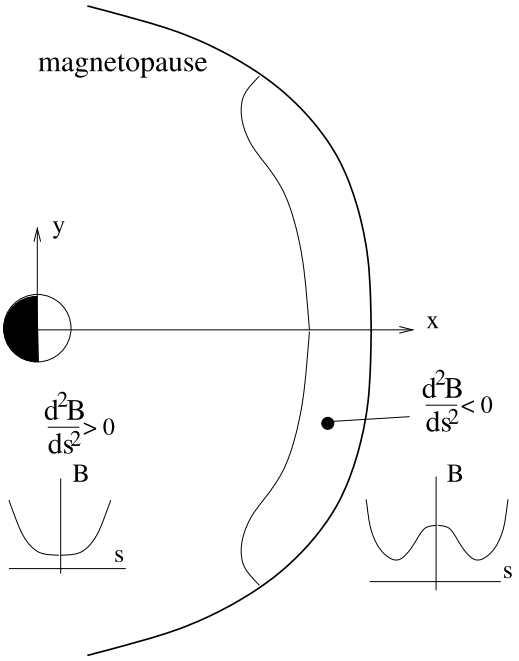

Figure 1. A schematic, equatorial picture of the region of interest in this paper. The coordinates are GSM. The region adjacent to the magnetopause has the property that the field lines that cross it have a local maximum of field strength there.

[1960], *Shabanskiy and Antonova* [1968], and *Roederer* [1970].

[6] The present study investigates the dynamics of particles that are initially bouncing on single-minimum field lines [U-shaped $B(s)$], but eventually drift onto double-minimum field lines [W-shaped $B(s)$]. If the drift path leads the particle onto a line whose local maximum is higher in value than the mirror field B_m, the bounce path will be broken. Figure 2 illustrates the effect of such a transition on particle motion.

[7] The full-particle trajectory shown in Figure 2 results from solving the relativistic Newton-Lorentz equation for an energetic (6.5 MeV) electron under Tsyganenko-89 [*Tsyganenko*, 1989] magnetic field model. Electric fields are ignored, along with any time dependence of the magnetic field. We have chosen an energetic electron merely for illustrative purposes; our discussion is not limited to energetic electrons and our theoretical results can be applied to any kind of bouncing particle with any energy, so long as the gyroradius is small compared to the scale length of the magnetic field.

[8] The electron starts its near-equatorial trajectory at local midnight and drifts adiabatically across local dawn. The motion conserves kinetic energy and the first invariant at all times; hence the mirror field is constant for each bounce. After a certain point near local noon, the bounce motion becomes confined to the Southern Hemisphere (another particle on the same drift shell, but with a different

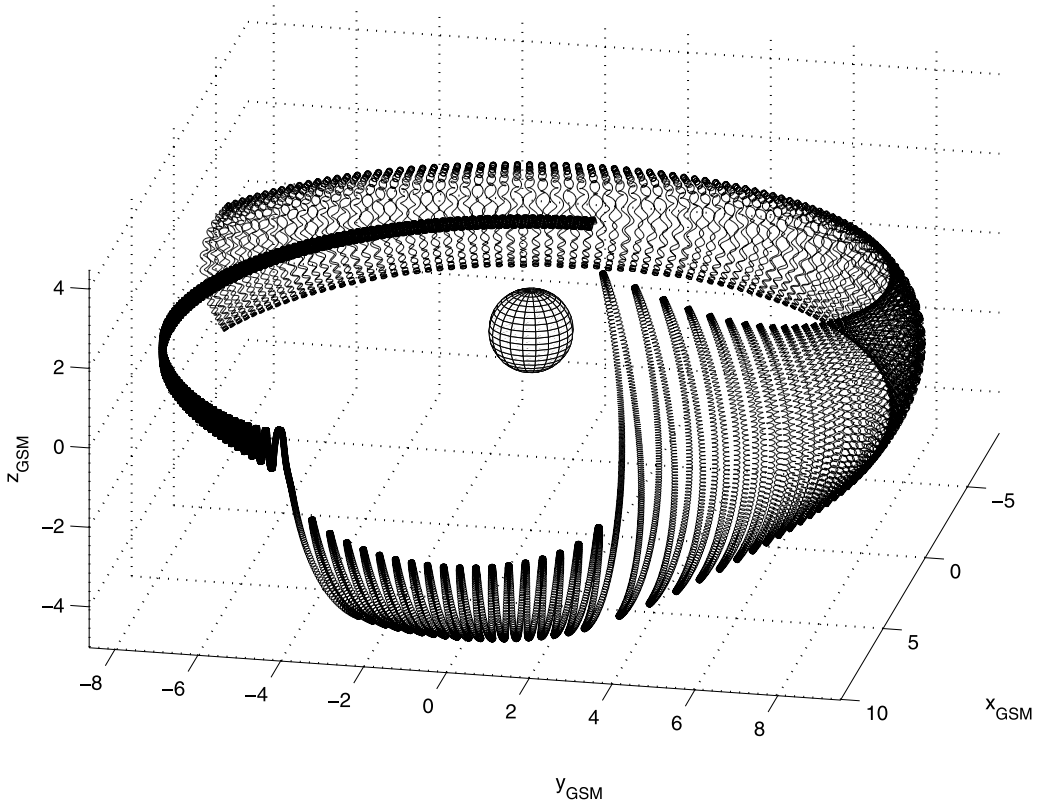

Figure 2. Trajectory of a 6.5-MeV electron in a Tsyganenko-1989c model. The particle is initiated at local midnight with a large equatorial pitch angle. The central sphere represents Earth, and the coordinates are in GSM system. Electric fields are ignored; the kinetic energy and the first invariant are constant along the motion.

bounce phase, would be diverted to the Northern Hemisphere). Past local noon, the drift motion carries the particle back onto dipole-like field lines so that the equator-centered bounce motion is resumed. However, as one can infer from the significantly different bounce amplitude, the value of the second invariant has changed and the particle is carried onto another drift shell.

[9] This transition is an example of "pitchfork bifurcation", where a single stable equilibrium point branches off into two stable and one unstable equilibria when a system parameter is varied (here, the local time). Hence we call this process drift-shell bifurcation (DSB). The purpose of this article is to quantify the second-invariant change due to DSB.

[10] Over a bifurcating drift shell, the particle motion is adiabatic everywhere, except for one or two bounce oscillations in the neighborhood of the "bifurcation lines". On these lines, the equation $B(s_m) = B_m$ is satisfied at exactly three mirror points: one point near the equatorial plane where the field strength is maximum, and two points to the north and south of it. For a given drift shell, there are two bifurcation lines located at either side of the local noon. *Northrop* [1963] qualitatively points out that, near the bifurcation lines, the central peak of $B(s)$ causes the parallel motion to slow down. Therefore the bounce period grows, and thus the adiabaticity conditions are temporarily violated, causing the second invariant to break (the cyclotron motion is not disturbed in this process, so the first invariant is not broken). In contrast, *Shabansky* [1971] argues that the bifurcation is so abrupt that the change in the second invariant due to the nonadiabatic effects can be ignored. At local noon the second invariant is exactly halved (for symmetric fields) and when the particle is back at the nightside, the second invariant value is back to its initial level.

[11] Perturbative analysis, presented in following sections, shows that the average nonadiabatic change predicted by Northrop is a small correction (averaged over all bounce phases), in the same order as the ratio of drift speed to bounce speed. Therefore the Shabansky argument holds to zeroth order in this parameter. For energetic and near-equatorial particles; however, the first-order correction can be significantly large. Figure 2 is a case in point.

[12] In choosing the theoretical approaches, we were guided by the studies of *Antonova et al.* [2003] and *Vainshtein et al.* [1999]. However, our work combines the two methods and it provides a more general treatment instead of using a specific magnetic field model.

[13] The bifurcating orbits we describe here should not be confused with the cusp-trapped orbits described by *Sheldon et al.* [1998], which are also found in the cusp region. Bifurcating orbits follow an Earth-centered drift shell at all times, while cusp-trapped orbits follow a drift path centered around the cusp axis, and have a much lower mirror field value. Under static conditions, the two types of orbits are topologically disconnected: There is no exchange between the two populations unless the kinetic energy and/or the first invariant is subject to change.

[14] The nonadiabaticity of DSB orbits, with sudden changes in a particle's second invariant as it passes each critical point, resembles another problem that is familiar in radiation-belt physics, namely the jumps that occur in the first invariant of a trapped particle when it passes through a resonance with a monochromatic wave [e.g., *Albert*, 1993].

2. Conditions for Bifurcation

[15] For clarity of discussion, we simplify the bifurcation problem without sacrificing its essence. We assume a magnetosphere that has both north-south and dawn-dusk symmetry. We further assume that the magnetic field is constant in time and electric fields are negligible. We also require that the particle has a sufficiently small gyroradius so that the first invariant is conserved, at least around the bifurcation lines.

[16] When there are no external forces, the quantity

$$I \equiv \int_{-s_m}^{s_m} \sqrt{1 - \frac{B(s)}{B_m}}\, ds \tag{1}$$

can be used as the second invariant of the motion. The mirror field B_m can be expressed as:

$$B_m = \frac{m v^2 \gamma^2}{2\mu} \tag{2}$$

where m is the mass of the particle, v is its speed, $\gamma \equiv (1 - v^2/c^2)^{-1/2}$ is the relativistic factor, and μ is the first invariant. The quantity I is related to the formal second invariant $J \equiv \oint p_{\|} ds$ by $I = J/2p$; therefore, J and I are both adiabatic invariants if the particle's kinetic energy is constant.

[17] Under the static conditions we assumed, I and B_m uniquely determine a drift shell. Furthermore, because I is defined in terms of field geometry, the drift path can be determined without referring to the dynamical details of the particle motion [*Roederer*, 1970]. (Of course, the initial conditions of the motion are necessary to evaluate I and B_m in the first place.) Then, using the initial conditions, we can predict whether DSB will occur or not.

[18] Suppose we initialize the particle with B_m and I. In order to determine the bifurcation line, consider the equatorial plane, which, by symmetry, contains all points with maximum $B(s)$ (in the absence of north-south symmetry, the discussion applies to the $\frac{dB}{ds} = 0$ surface). Furthermore, consider the contour $\mathcal{C}(B_m) = \{(x,y)|\ |\mathbf{B}(x,y,z=0)| = B_m\}$, which is a contour of constant field strength on that plane. The bifurcation point, the location where the bifurcation line intersects the equatorial plane, must lie on $\mathcal{C}(B_m)$.

[19] For the field line that perpendicularly crosses the bifurcation region at point (x,y), we define the quantity

$$\Upsilon(x,y) \equiv 2 \int_0^{s_m} \sqrt{1 - \frac{B(s)}{B(0)}}\, ds \tag{3}$$

where $B(s)$ is defined along that particular field line and s_m is defined by $B(s_m) = B(0)$ (we set the origin $s = 0$ to the location where $\frac{dB}{ds} = 0$). Note that Υ has the same form as the second invariant integral [equation (1)]. Its value is zero at the edge of the bifurcation region and increases toward the magnetopause. Bifurcation occurs when the particle drifts to a point where $\Upsilon(x,y) = I$, whose location can be determined

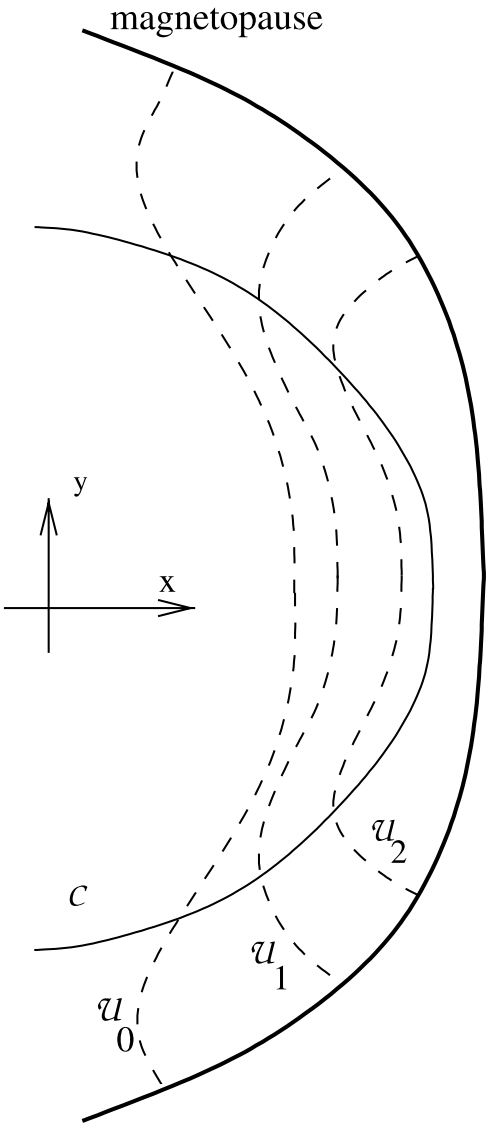

Figure 3. A schematic view of the bifurcation region in the equatorial plane. Curve $\mathcal{C}$ is a contour of constant B_m, and $\mathcal{U}_0, \mathcal{U}_1, \mathcal{U}_2$ are curves of constant Υ. The intersection of $\mathcal{C}$ with $\mathcal{U}_i$ gives the bifurcation points for the relevant drift shell.

to arbitrary accuracy by searching along the contour $\mathcal{C}(B_m)$. Electron drift shells bifurcate on the dawn side, ion drift shells on the dusk side.

[20] Let $\mathcal{U}(I) = \{(x,y)|\Upsilon(x,y) = I\}$ be the equatorial contour of constant Υ. For a drift shell defined by I and B_m, the bifurcation points are given by the intersection of $\mathcal{U}(I)$ and $\mathcal{C}(B_m)$. Both curves can be computed easily for a given magnetic field model. Figure 3 presents a generic view of how these curves are located on the equatorial plane. Curves $\mathcal{U}_0$, $\mathcal{U}_1$, $\mathcal{U}_2$ correspond to I_0, I_1, I_2, respectively, with $I_0 < I_1 < I_2$. The figure shows that the bifurcation point is closer to local noon for shells with larger second invariant, keeping the mirror field constant.

[21] By extrapolation of this argument we can see that at a certain value $I = \mathcal{I}$, the curve $\mathcal{U}(\mathcal{I})$ becomes tangential to $\mathcal{C}(B_m)$, and for $I > I$, there is no intersection at all as illustrated by curves $\mathcal{C}_1$ and $\mathcal{U}_2$ in Figure 4. Thus for a given B_m, there exists an upper limit $\mathcal{I}(B_m)$ such that shells with $I > \mathcal{I}(B_m)$ do not bifurcate. This maximum value is equal to the value of Υ evaluated at the point where $\mathcal{C}(B_m)$ intersects local noon.

[22] On the other hand, for shells with mirror fields less than the subsolar field, $B_{subsolar}$, such a maximum value does not exist. The contour $\mathcal{C}_2 = \mathcal{C}(B_{m2})$ in Figure 4 does not pass through local noon but joins the magnetopause surface. It can be seen that for any I, $\mathcal{U}(I)$ must intersect $\mathcal{C}_2$; therefore, there is no limiting second-invariant value for the existence of DSB for low values of B_m.

[23] For both types of contours, however, it is possible to initialize the particle with such a large second invariant that it will not enter the bifurcation region, but drifts directly into the magnetopause. The subsequent dynamics of such "quasi-trapped" particles are outside the scope of this study (see, *Young et al* [2002] for the violation of

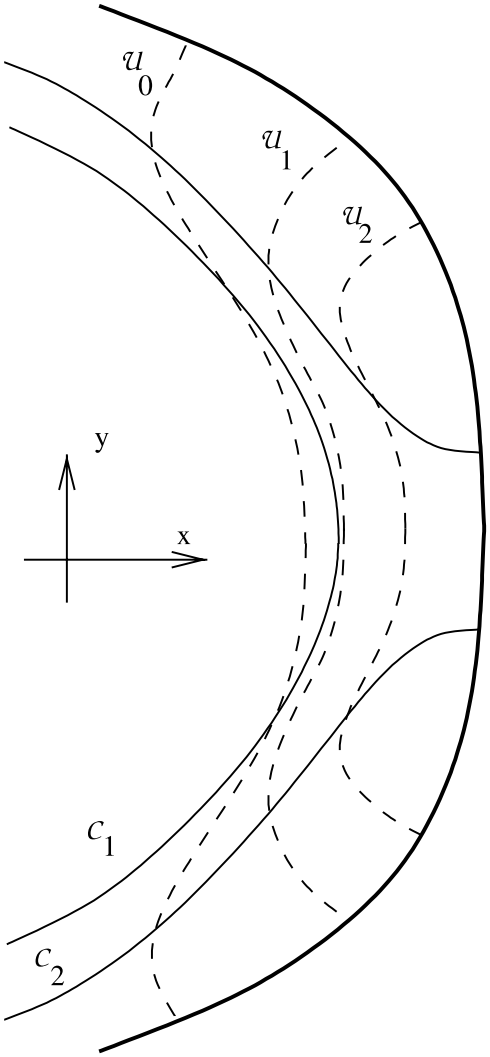

Figure 4. Existence of a maximum I for bifurcation. Given B_{m1} such that $\mathcal{C}_1 = \mathcal{C}(B_{m1})$, the curve $\mathcal{U}_2 = \mathcal{U}(I_2)$ does not intersect $\mathcal{C}_1$, so there is no bifurcation. For smaller $B_{m2} < B_{subsolar}$ such that $\mathcal{C}_2 = \mathcal{C}(B_{m2})$, all $\mathcal{U}$ curves must intersect $\mathcal{C}_2$, so DSB always occurs.

the first invariant that occurs when a particle crosses the magnetopause).

3. Sensitive Dependence on Bounce Phase

[24] In the first section we demonstrated that DSB can influence the second invariant significantly. Here we illustrate how this change occurs, and how it depends on the bounce phase of the particle at the bifurcation line. We defer the mathematical analysis to the following sections; this section's material consists of simulated trajectories.

[25] Such dependence on bounce phase is reported in several earlier studies, which follow test-particle trajectories under a variety of magnetospheric configurations, for example, *Orloff* [1998] (protons under integrated space-weather model) and *Delcourt and Sauvaud* [1998,1999] (kiloelectron volt protons under Tsyganenko-89 and Mead-Fairfield model, respectively). Here we present a more systematic study of phase-dependence by constructing a bounce-phase ensemble that finely samples the phase interval.

[26] All test-particle trajectories in this section are produced by solving the guiding-center equations of motion under a double-dipole model. The guiding-center approximation is theoretically expected to be valid because the nonadiabaticity at the bifurcation line should not break the first invariant, and we have verified that expectation by numerical integration of full-particle trajectories. The double-dipole model consists of two Earth-strength dipoles, moments parallel, placed with a distance 20 R_e between them so that the magnetopause is simulated as a plane at half distance 10 R_e [see, *Chapman and Bartels*, 1940]. This is one of the simplest magnetic configuration that allows for DSB; its simplicity makes it convenient for fast simulations and for analysis by computer algebra systems. We emphasize that the general features of DSB discussed in this study are not limited to this simple model. The theory we present in later sections is applicable to a wide variety of magnetospheric models.

[27] We construct a set of initial conditions such that they are all located on the same drift shell, but differ in bounce phase. One way of producing this set is to consider an initial guiding line ℓ and choosing some points on it. Let $P_i = (x_i,y_i,z_i)$ be one initial position and B_m be the mirror field value. Because all members of the initial condition set must have the same value for the first invariant and for the energy, the pitch angle at the initial position P_i must satisfy $B(x_i,y_i,z_i) = B_m \sin^2\alpha_i$. Furthermore, the bounce phase ϕ_i at P_i is given by:

$$\phi_i - \phi_0 = \pi \frac{\int_{s_0}^{s_i} \left(1 - \frac{B(\sigma)}{B_m}\right)^{-1/2} d\sigma}{\int_{-s_m}^{s_m} \left(1 - \frac{B(\sigma)}{B_m}\right)^{-1/2} d\sigma} \quad (4)$$

where ϕ_0 is the phase assigned to the reference point s_0, and s_i is the arc length at P_i.

[28] We initiate one hundred trajectories of electron guiding-centers at various points $\{P_i\}$ on ℓ and follow them until they cross the bifurcation region, recording the second invariant values for each trajectory. We choose an arbitrary initial guiding line that passes through the point $P_0 = (7\ R_e, -7\ R_e, 0)$. Zero phase is assigned to the point P_0. We set up the ensemble such that the equatorial pitch angle at P_0 is 80°, and the electrons have 175 keV kinetic energy. The initial second invariant has the value $I_0 = 0.45\ R_e$, and the mirror field is $B_m = 42.9$ nT.

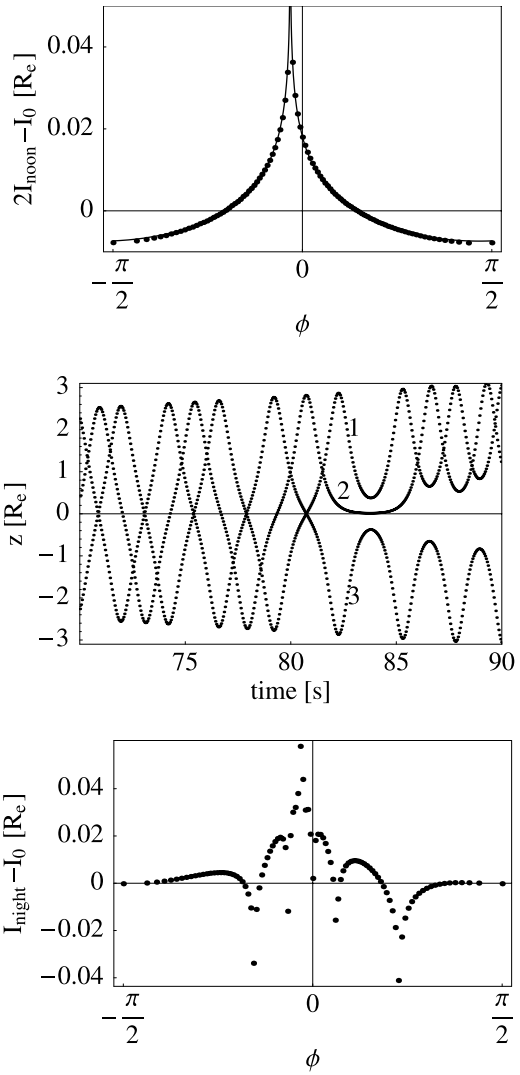

Figure 5. Top: The change in the second invariant after DSB, versus the bounce phase. Middle: The motion $z(t)$ for selected trajectories. (1) Corresponding to phase $-\pi/2$, (2) corresponding to the phase near the peak of the curve, and (3) phase $\pi/2$. Bottom: The total change after crossing the conjugate bifurcation line.

[29] Figure 5 displays how the change of the second invariant due to DSB depends on the bounce phase of each particle. The top panel shows the effect of a single bifurcation, when the particles are near local noon. We see that the difference $2I_{noon} - I_0$ is negative for some particles, and positive for others. The narrow spike in the plot indicates that a few of them acquire significantly large second invariant values.

[30] With hindsight (see following sections), we fit the data to a curve in the form $a + b\ln|2\sin(\phi - c)|$. The continuous curve in the top panel of Figure 5 is a fit with $a = 2.85\times10^{-4}$, $b = -0.011$, $c = -0.101$. The ensemble

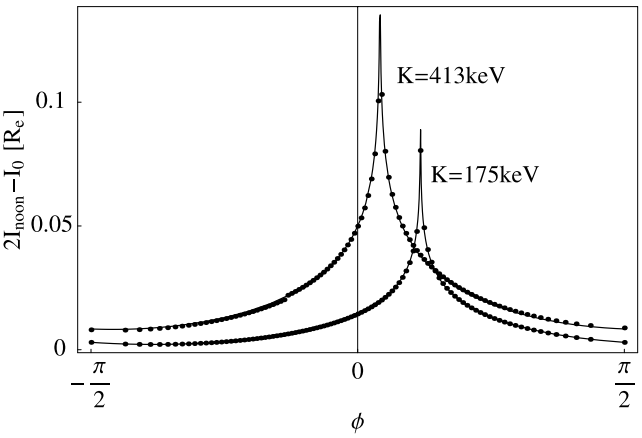

Figure 6. Two more bounce-phase ensembles at the same starting location as in Figure 5, with $\alpha_{eq} = 89.5°$. In both ensembles, the dayside second invariant has increased for all particles. The increase is more significant with the energetic ensemble. The continuous lines are nonlinear fits to the points.

average of the curve (average over ϕ) is equal to the parameter a, which is very close to zero.

[31] The middle panel, which shows the trajectories for three members of this ensemble, hints at the mechanism that causes the sharp increase at some phases. The orbits labeled 1 and 3 correspond to particles with phases $-\pi/2$ and $\pi/2$, respectively, and orbit 2 corresponds to the phase closest to the peak of the top panel. We see that orbit 2 lingers around the equator much longer than orbits 1 and 3 do, thus breaking the second invariant. The particle just reaches the peak when the magnetic field there reaches B_m, and the parallel motion is therefore stalled. Meanwhile, due to drift, the side minima of the potential $B(s)$ become deeper so that when the particle finally falls to one side, the orbit goes through a lower field minimum, thus acquiring a larger second invariant. If we sample the peak more finely, we can find other orbits that come closer to equator and stall for longer times.

[32] When the members of the initial ensemble are scattered onto neighboring drift shells, they drift across the day side with slightly different speeds. We follow the trajectories until they cross the conjugate bifurcation line and return to the night side. The bottom panel of Figure 5 shows the difference between final and initial second invariants versus the initial bounce phase. The plot displays the same central peak as the plot of the top panel, but it is scrambled because of the speed differential among the particles. The downward pointing sharp peaks result from the same "hang-up" process that creates the peak of the top panel, working backwards in this case. A finer sampling reveals further dips around the main upward peak (not shown); in the continuum limit, one can expect to find an infinite number of dips, very close to each other.

[33] We construct a second and a third ensemble, using the same initial guiding line. In the second ensemble we increase the equatorial pitch angle to 89.5°, setting the kinetic energy of electrons again to 175 keV. The mirror field of the ensemble is now $B_m = 41.88$ nT, almost the same as that of the first ensemble; however, now the initial second invariant value is set to the small value $I_0 = 0.0012\ R_e$. The third ensemble also has an equatorial pitch angle of 89.5°, but the kinetic energy of each member is increased to 413 keV.

[34] Figure 6 displays the change in the second invariant after a single bifurcation of the original drift shell of these ensembles. The change ΔI is positive for all members of the ensemble, and larger for the ensemble with higher kinetic energy.

[35] The function $a + b\ln|2\sin(\phi - c)|$ with $a = 0.011$, $b = -0.012$ and $c = 0.370$ provides a very good fit to the data points of the second ensemble. A similarly good fit for the third ensemble is given with the parameters $a = 0.023$, $b = -0.021$, and $c = 0.131$. In these examples, the ensemble-averaged change of the second invariant is not zero, but significantly large and positive.

4. Nonequatorial Particles

[36] In this section and the following, we present a theoretical analysis of the nonadiabatic changes imposed by DSB. This section applies the theory of separatrix crossing to the problem in order to determine the change in the second invariant. This method was applied to space-plasma problems before: In their well-known study, *Büchner and Zelenyi* [1989] apply the theory of separatrix crossing to the analysis of Speiser orbits in the magnetotail. In that problem, the action that is affected by the crossing is not the second invariant, but $\oint \dot{z}dz$, which is similar to the first invariant. Although Speiser orbits are very different from bifurcating orbits, the same formalism applies to both.

[37] The study by *Antonova et al.* [2003] has a scope that significantly overlaps with the present section. The authors apply separatrix-crossing theory to the DSB problem, and obtain analytical results for a specific magnetic field. Their results have the same properties as the results we present here. The present study differs from the work by Antonova et al. mainly in two aspects. We do not presuppose a specific magnetic field, so our results are applicable to a wide class of models; also, we present a treatment of equatorial particles whose bifurcation cannot be analyzed with separatrix-crossing theory.

[38] A good review of the adiabatic invariant and of separatrix crossing, including some applications, is provided by *Henrard* [1993].

4.1. Separatrix-Crossing Theory

[39] Using the guiding-center formalism, the bounce problem can be expressed in the simple form:

$$\frac{d^2 s}{dt^2} = -\frac{\mu}{\gamma^2 m}\frac{dB}{ds} \tag{5}$$

Here μ and γ are constants by our assumptions, and $B(s)$ is a slowly changing function (due to drift onto other guiding lines). Also, the equation undergoes bifurcation at some instant. In that form, there is no known explicit solution to equation (5), even when one expands $B(s)$ in a Taylor series. However, we are mainly interested in the relation between initial and final values of the second invariant (essentially an average quantity), and not in the details of the particle trajectory. To obtain such a relation, we can use the

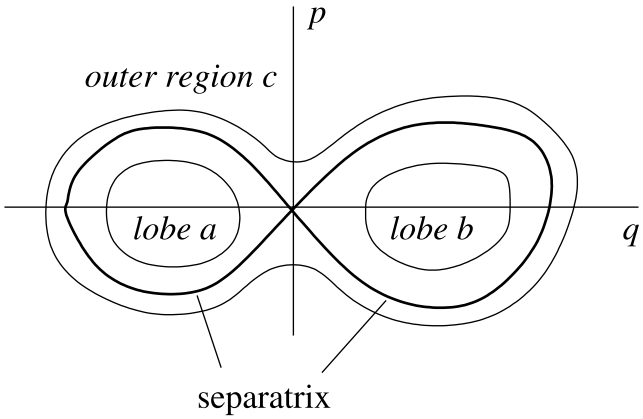

Figure 7. The generic contours of the Hamiltonian equation (6). The separatrix corresponds to the contour $H = 0$. Contours with negative H are confined to the lobes (region a or b), while positive H contours go around both lobes (region c).

separatrix crossing theory developed by *Cary et al.* [1986] (CET).

[40] CET postulate the dimensionless Hamiltonian:

$$H(q,p;\lambda) = \frac{\omega}{2}\left(p^2 - q^2\right) + \delta H(q,p;\lambda) \tag{6}$$

which depends on the slowly changing parameter λ ($\dot{\lambda} \equiv \varepsilon \ll 1$ for all times). The parameter ω does not depend on q or p, but may depend on λ. The term δH contains higher powers of q and p, so that δH is negligible near the origin.

[41] Figure 7 shows the contours of H at fixed λ (the frozen system), which are also the phase-space orbits of the system. The origin ($q = 0$, $p = 0$) is a saddle point, and the separatrix curve corresponds to the $H = 0$ contour. Orbits with positive H go around the separatrix, while those with negative H are confined into one of the separatrix lobes.

[42] The parameter ω can be intuitively interpreted as the exponentiation rate of the trajectories near the saddle point at the origin. To see this, note that near the origin, δH is ignored and the solution to the resulting Hamiltonian describes orbits with $q(t), p(t) \propto e^{\pm\omega t}$.

[43] Let $Y_a(\lambda)$ and $Y_b(\lambda)$ be the phase space area inside the left and the right lobe of the separatrix, respectively. Consider an orbit that is initially outside the separatrix, with action J_0. If $Y_a(\lambda)$ and/or $Y_b(\lambda)$ are slowly and monotonically increasing, then there will come a time λ_x where $Y_a(\lambda_x) + Y_b(\lambda_x) = J_0$, and the orbit crosses the separatrix. The crossing occurs essentially because the lobe area shrinks at a rate that is $\mathcal{O}(\varepsilon)$, while the area J_0 inside the trajectory shrinks much more slowly (due to adiabatic invariance), so the separatrix catches up with the trajectory. Conversely, if the orbit is initially inside lobe a, whose area is shrinking, crossing occurs when $Y_a = J_0$.

[44] The analogy between this problem and DSB is straightforward: J_0 corresponds to the initial second invariant, the total lobe area $Y_a(\lambda) + Y_b(\lambda)$ corresponds to Υ and the crossing time λ_x corresponds to the location of the bifurcation line.

[45] CET adopt a perturbative approach to relate the postcrossing action J_f to the initial action. The small perturbation parameter is $\varepsilon \equiv \dot{\lambda}$. In the final result, terms of order ε^2 or higher are ignored.

[46] When the Hamiltonian [equation (6)] is symmetric in q and p, both lobes cover equal areas and these areas have equal rates of change ($Y_a = Y_b \equiv Y$, $\dot{Y}_a = \dot{Y}_b \equiv \dot{Y}$). In this case, the change in the action for an orbit that is initially outside of either lobe is:

$$J_f = Y(\lambda_x) - \left.\frac{\dot{Y}}{\omega}\right|_{\lambda_x} \ln|2\sin\phi| + \mathcal{O}\left(\varepsilon^2\right) \tag{7}$$

where ϕ is a constant depending on initial conditions. The dependence on the initial action J_0 is implicit in λ_x, via $2Y(\lambda_x) = J_0$. For an orbit that is initially inside a lobe that is shrinking, the relation is:

$$J_f = 2Y(\lambda_x) - 2\left.\frac{\dot{Y}}{\omega}\right|_{\lambda_x} \ln|2\sin\phi| + \mathcal{O}\left(\varepsilon^2\right) \tag{8}$$

[47] In these expressions, the first term is $\mathcal{O}(1)$ and the second term is $\mathcal{O}(\varepsilon)$ (because $\dot{Y} = \varepsilon \frac{dY}{d\lambda}$). In the limit $\varepsilon \to 0$ (for example, infinitely fast bounce motion) the correction term can be omitted; furthermore, if $Y(\lambda)$ initially increases and then decreases, we see that after a conjugate pair of crossings, the action is back to its initial value. This is equivalent to the argument of *Shabansky* [1971] mentioned before.

[48] The crossing parameter ϕ is directly related to the phase of the motion far from the separatrix. The function $-\ln|2\sin\phi|$ is sharply increasing near $\phi = 0$ and $\phi = \pi$, and shallow in between. Initial conditions corresponding to $\phi \approx 0$ (or an integer multiple of π) create orbits whose action is significantly increased. They are the orbits which spend a considerable time near the saddle point (cf. Figure 5).

[49] If a set of initial conditions is uniformly distributed in the angle variable but have a common value of J_0, they are uniformly distributed in ϕ, too. The average of the jumps of the second invariant for such an ensemble will be equal to zero, because $\int_0^{2\pi} \ln|2\sin\phi|\, d\phi = 0$. However, the root mean square deviation is not zero, which means that the members of the ensemble are scattered onto neighboring orbits.

[50] The results in equations (7) and (8) for the postcrossing action are valid only when $J \gg \varepsilon$, because the perturbation series is cut off after first order. When $J \sim \varepsilon$, crossing takes place as soon as the separatrix comes into existence. For the DSB problem, this requirement means that equatorial particles with $I \approx 0$ are excluded from this analysis. The case of very small initial second invariant is analyzed in section 5.

[51] The interested reader can check the theory against numerical experiments with a toy problem. The quartic Hamiltonian

$$H(q,p,\lambda) = \frac{p^2}{2} - \lambda\frac{q^2}{2} + \frac{q^4}{4} \tag{9}$$

where $\lambda = \varepsilon t$, provides a test case, which can be used to gain an intuition for the separatrix crossing problem. To

have repeated separatrix crossings, just like it occurs with DSB, one can set λ to vary periodically in slow time, for example, $\lambda = c_0 + c_1\sin(\varepsilon t)$, where c_0 and c_1 are constants.

4.2. Application to Drift-Shell Bifurcation

[52] In order to apply the theory of separatrix crossings to the DSB problem, we postulate the following bounce Hamiltonian:

$$H(s, v_\parallel; \lambda) = \frac{v_\parallel^2}{2} + \frac{\mu}{\gamma^2 m}(B_\lambda(s) - B_\lambda(0)) \tag{10}$$

where $v_\parallel = \dot{s}$, and λ is a slowly changing coordinate along the drift path. This Hamiltonian function gives the same equation of motion as equation (5). The constant term $\mu B\lambda(0)/\gamma^2 m$ ensures that the separatrix corresponds to the $H = 0$ contour. Finally, the Taylor expansion

$$B_\lambda(s) - B_\lambda(0) = -\left|\frac{\mathrm{d}^2 B_\lambda}{\mathrm{d}s^2}\right|_{s=0} \frac{s^2}{2} + \mathcal{O}(s^4) \tag{11}$$

shows that the bounce Hamiltonian is directly compatible with the assumed form [equation (6)] of CET theory (because of the north-south symmetry, the expansion has no terms with odd powers).

[53] The dimensionless Hamiltonian equation (6) is related to equation (10) by a scale transformation; therefore the action J calculated from equation (6) is related to the second invariant I by a constant factor. Then, when adapting the jump relations (7) and (8), we can substitute I for J and Υ / 2 for Y, and the constant factors will cancel.

[54] From the lowest-order terms of the bounce Hamiltonian equation (10) we determine the exponentiation rate as:

$$\omega(\lambda) = \sqrt{\frac{\mu}{\gamma^2 m}\left|\frac{\mathrm{d}^2 B_\lambda}{\mathrm{d}s^2}\right|_{s=0}} \tag{12}$$

[55] In the present problem the change of the lobe area is caused by the slow drift, then the rate of change of Υ is given by the directional derivative:

$$\frac{\mathrm{d}\Upsilon}{\mathrm{d}t} = \langle \mathbf{v}_D \rangle \cdot \nabla\Upsilon \tag{13}$$

Here $\langle \boldsymbol{v}_D \rangle$ is the bounce-averaged drift velocity; therefore, $\dot{\Upsilon}$ is equal to the spatial derivative of Υ in the drift direction at the bifurcation line. Then, for a particle that enters the bifurcation region with initial (nightside) second invariant I_0, first invariant μ and crossing parameter ϕ_0, the new second invariant value I_1 will be:

$$I_1 = \frac{I_0}{2} - \frac{1}{2}\left[\left(\frac{\mu}{\gamma^2 m}\left|\frac{\mathrm{d}^2 B}{\mathrm{d}s^2}\right|_{s=0}\right)^{-1/2} \langle \boldsymbol{v}_D \rangle \cdot \nabla\Upsilon\right]_{\ell_b} \times \ln|2\sin\phi_0| \tag{14}$$

All factors are evaluated at the bifurcation line ℓ_b, which is the magnetic field line that goes through point $(x_\mathrm{b}, y_\mathrm{b})$ satisfying $I_0 = \Upsilon(x_\mathrm{b}, y_\mathrm{b})$.

[56] The branches of the drift shell come together at the conjugate bifurcation line ℓ'_b, located at $(x'_\mathrm{b}, y'_\mathrm{b})$ satisfying $I_1 = \Upsilon(x'_\mathrm{b}, y'_\mathrm{b})$. When the particle crosses it with crossing parameter ϕ_1, the new nightside second invariant value is:

$$I_2 = 2I_1 - \left[\left(\frac{\mu}{\gamma^2 m}\left|\frac{\mathrm{d}^2 B}{\mathrm{d}s^2}\right|_{s=0}\right)^{-1/2} \langle \mathbf{v}_D \rangle \cdot \nabla\Upsilon\right]_{\ell'_b} \times \ln|2\sin\phi_1| \tag{15}$$

[57] The results in equations (14) and (15) are quite versatile, and they can be applied to any magnetic field model with north-south symmetry (dawn-dusk symmetry is not necessary). Given the initial first and second invariants and the energy of a particle at the night side, the jump magnitude (the phase-independent factor in brackets) can be predicted from the magnetic geometry alone, without following the actual particle trajectory.

[58] Furthermore, the results are applicable even when time-dependence is allowed, even though I is not an invariant when the speed of the particle is changing. If the changes imposed by time-dependent magnetic field and/or electric fields are adiabatic, one can use the relevant conservation relations to follow the drift shell up to the bifurcation line and calculate the new second invariant using the instantaneous values of μ, I, and v.

[59] The crossing parameter ϕ depends on the details of the bounce motion, so it requires following the actual path of the system (the conservation laws are not sufficient to specify it). At the first bifurcation, an ensemble of initial bounce phases will map onto an ensemble of ϕ, plus a constant shift. Members of the ensemble are scattered onto slightly different drift shells with slightly different drift speeds. It takes many bounces until they reach the next bifurcation line, by which time the initial bounce phases are thoroughly mixed. Therefore in the case of multiple crossings we use the random phase approximation, and set ϕ randomly, which assumes that there are no correlations between the two crossings. This assumption is not strictly true: *Cary and Skodje* [1989] show that from one crossing to the next, phase mixing is not perfect and correlations persist; however, *Bazzani* [1999] demonstrates that after a few crossings, phase mixing becomes complete and correlation between the initial and current phases goes to zero.

4.3. Numerical Study

[60] We can express equation (14) in a more useful form by approximating the bounce-averaged drift velocity $\langle v_\mathrm{D} \rangle$ with the pure gradient drift velocity $\boldsymbol{v}_\mathrm{G}$:

$$\langle \mathbf{v}_\mathrm{D} \rangle \approx \mathbf{v}_\mathrm{G} = \frac{\gamma m v^2}{2|q|B_\mathrm{m}^2}\,\mathrm{sgn}(q)\hat{b} \times \nabla_\perp B \tag{16}$$

[61] This approximation is reasonably good for particles with large equatorial pitch angles; however, it does not hold for all bifurcating particles (as described in section 2, under some conditions, particles with any pitch angle can bifurcate). Still, the gradient drift is always a significant component of the overall drift; therefore the approximation provides at least an order-of-magnitude estimate.

[62] Using this approximation, and substituting $\mu / (\gamma^2 m) = v^2 / (2B_\mathrm{m})$, equation (14) can be rewritten as:

$$2I_1 - I_0 = \frac{\gamma m v}{|q|B_\mathrm{m}} \cdot G \cdot (-\ln|2\sin\phi_0|) \tag{17}$$

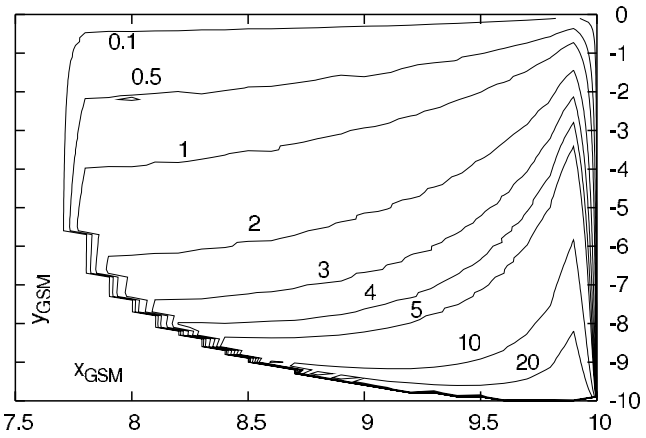

Figure 8. Curves of constant G under double-dipole magnetic field. The magnetopause is the $x = 10$ plane (the right-hand edge of the figure). The number $G(x,y)$ is a measure of the violation of the second invariant for a drift shell that bifurcates at point (x,y). For most of the bifurcation region the value of G is of the order of one.

where

$$G \equiv \mathrm{sgn}(q)\left[\frac{\hat{b}\times\nabla_{\perp}B}{\sqrt{2B_{\mathrm{m}}|B''|}}\cdot\nabla\Upsilon\right]_{(x_{\mathrm{b}},y_{\mathrm{b}})} \tag{18}$$

We recognize that the first factor $\gamma mv/(|q|B_{\mathrm{m}})$ is equal to ρ_{m}, the gyroradius at the mirror point. The dimensionless factor G should be evaluated right at the bifurcation point $(x_{\mathrm{b}}, y_{\mathrm{b}})$. The function $G(x,y)$ is unique to a given magnetic field configuration and does not depend on the particle parameters. Hence one can calculate $G(x,y)$ in advance, perhaps on a grid that spans the bifurcation region, and then evaluate $G(x_{\mathrm{b}},y_{\mathrm{b}})$ for the specific bifurcation point dictated by the particle's initial conditions.

[63] In this form, we also see that ρ_{m} gives the scale of the change in the second invariant. For most bounce phases, the phase-dependent factor $-\ln|2\sin\phi_0|$ is of order 1. Furthermore, we demonstrate below that the dimensionless geometric factor G is of order 1 for most of the bifurcation region. Therefore the change $2I_1 - I_0$ is of the order of a few ρ_{m}. This result is not surprising because $\rho_{\mathrm{m}}/R_{\mathrm{e}}$ is the small parameter of the system and the perturbative analysis keeps terms up to $\mathcal{O}(\rho_{\mathrm{m}}/R_{\mathrm{e}})$.

[64] At any given equatorial point (x,y) in the bifurcation region, the value of $G(x,y)$ can be calculated as follows: We follow the field line passing through the point and evaluate the second derivative of $B(s)$ along it by finite differences. The direction vector $\hat{b}$ is in z-direction because of the equatorial symmetry. The mirror field B_{m} will be equal to the field strength at (x,y) because this point is a bifurcation point. The gradients $\nabla_{\perp} B$ and $\nabla\Upsilon$ can be evaluated by taking finite differences along x and y directions around the point.

[65] Using this procedure, we have evaluated $G(x,y)$ over a grid of equatorial points over a region that spans the bifurcation region. Figure 8 shows the contour plot of $G(x,y)$ for the double-dipole model that is used to produce the simulated trajectories of section 3.

[66] We can directly check the theoretical prediction against the first set of synthetic data in section 3. The fit

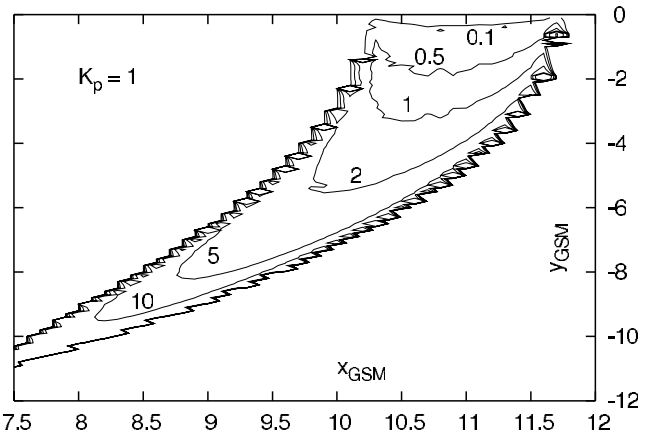

Figure 9. Curves of constant G under Tsyganenko-1989c magnetic field model, with parameter $K_p = 1$ (low activity).

to the data in Figure 5 shows that the coefficient of the logarithmic term is -0.011; hence, $\rho_{\mathrm{m}}G = 0.011\ R_{\mathrm{e}}$. The mirror gyroradius of the followed particle is $\rho_{\mathrm{m}} = 5.58\times10^{-3}\ R_{\mathrm{e}}$, which gives the "experimental" value $G = 1.97$ for the drift shell over which this particular ensemble moves.

[67] The bifurcation point for this particular drift shell is at $x_{\mathrm{b}} = 8.23\ R_{\mathrm{e}}$, $y_{\mathrm{b}} = -5.97\ R_{\mathrm{e}}$. Evaluation of G at this point, as defined in equation (17), gives $G = 1.90$ (cf. Figure 8), in good agreement with the numerical simulation.

[68] The method is directly applicable to more realistic magnetospheric models. Figures 9 and 10 show level curves of G under Tsyganenko-1989c model, with $K_{\mathrm{p}} = 1$ and $K_{\mathrm{p}} = 7$, respectively. We see that the range of G values and the shape of the contours are comparable to the double-dipole case. The similarity suggests that the fundamental qualities of DSB are common features of both simple and complicated models.

5. Equatorial Particles

[69] The CET theory of separatrix crossing outlined in the previous section, albeit powerful and applicable to a wide variety of systems, cannot be used when the initial action is very small. In the context of the DSB problem, application of CET theory requires that $I_0 \gg \rho_{\mathrm{m}}$. However, energetic

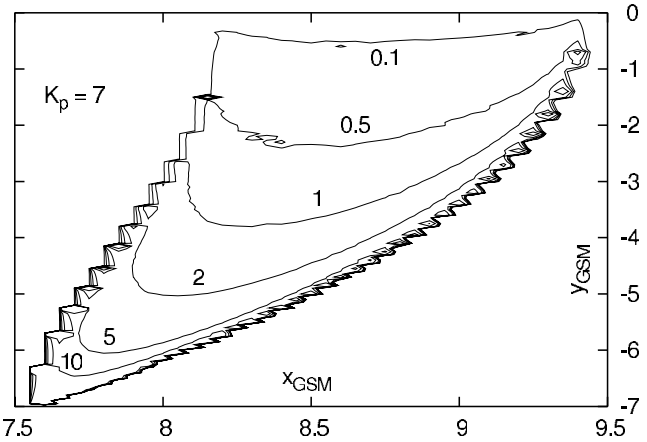

Figure 10. Curves of constant G under Tsyganenko-1989c magnetic field model, with parameter $K_p = 7$ (high activity).

particles (large ρ_m) with large equatorial pitch angles (small I_0) can easily violate this condition (for example, relativistic electrons with pitch angles >80°). To analyze these cases, we require a complementary approach that is valid in the regime of small I_0.

[70] Numerical traces of equatorial particles (i.e., very small initial action) show qualitative differences compared to nonequatorial particle traces. In particular, the bounce-phase-ensemble graphs in Figure 6 show that the ensemble average of the second invariant change is nonzero. This observation generally holds for similar bifurcations [cf. *Bulanov and Naumova*, 1996 and *Chirikov and Vecheslavov*, 2000].

[71] In the context of space plasmas, this method was applied by *Vainshtein et al.* [1999] to Speiser orbits in the magnetotail. Their results are formally similar to ours, even though the system is very different.

5.1. Bounce Motion With Small Amplitude

[72] In order to develop an expression for the change of the second invariant with small I_0, we return to the bounce equation of motion [equation (5)]. Because the bounce amplitude is small, we can expand $B(s)$ in a Taylor series up to fourth order, resulting in:

$$\frac{\mathrm{d}^2 s}{\mathrm{d}t^2} = -\frac{\mu}{m\gamma^2}\left[-\left|B^{(2)}\right|s + \frac{B^{(4)}}{6}s^3\right] \tag{19}$$

where $B^{(2)} \equiv \left.\frac{\mathrm{d}^2 B}{\mathrm{d}s^2}\right|_{s=0}$ and $B^{(4)} \equiv \left.\frac{\mathrm{d}^4 B}{\mathrm{d}s^4}\right|_{s=0}$, and both derivatives are evaluated at the equator. The second derivative $B^{(2)}$ is negative. We will assume that $B^{(2)}$ is slowly changing with time due to drift, but the change of $B^{(4)}$ is negligible.

[73] Bifurcation will occur within a short distance into the bifurcation region (within one or two bounce cycles). Therefore we express the second derivative $B^{(2)}$ as a linear function of drift distance λ:

$$B^{(2)} = v_G \left.\frac{\mathrm{d}B^{(2)}}{\mathrm{d}\lambda}\right|_{\lambda=0} t \tag{20}$$

where we set the origin $\lambda = 0$ to the edge of the bifurcation region so that the constant term of $B^{(2)}$ vanishes. The directional derivative is evaluated along the contour of constant $B = B_m$ because this is the path of an equatorial particle, and the drift speed v_G is purely due to gradient drift. Thus we approximate the bounce problem as motion under a quartic potential with a linearly rising central peak:

$$\frac{\mathrm{d}^2 s}{\mathrm{d}t^2} = \underbrace{\frac{\mu v_G(\lambda=0)}{m\gamma^2}\left.\frac{\mathrm{d}\left|B^{(2)}\right|}{\mathrm{d}\lambda}\right|_{\lambda=0}}_{a} ts - \underbrace{\frac{\mu B^{(4)}}{6m\gamma^2}}_{b} s^3 \tag{21}$$

where a and b are positive constant parameters.

5.2. The Painlevé-II Equation

[74] The scale transformation $t \to a^{-1/3}x$, $s \to \sqrt{\frac{2}{b}}\, a^{1/3} y$ converts the bounce equation (21) into Painlevé's second equation:

$$\frac{\mathrm{d}^2 y}{\mathrm{d}x^2} = xy - 2y^3 \tag{22}$$

The six Painlevé equations hold a special place in the theory of second-order nonlinear ODEs [*Clarkson*, 2003]. Their solutions, the Painlevé transcendents, cannot be expressed in terms of the more familiar functions. However, the thoroughly investigated asymptotic solutions can be. In the limit $x \to -\infty$, *Its and Kapaev* [1988] give the following asymptotic result for the Painlevé-II equation:

$$y(x) \sim (-x)^{-1/4}\alpha \times \sin\left[\frac{2}{3}(-x)^{3/2} + \frac{3}{4}\alpha^2 \ln(-x) + \varphi\right] \tag{23}$$

The solution parameters $\alpha > 0$ and $0 \le \varphi < 2\pi$ depend on initial conditions. In the opposite limit, as $x \to \infty$:

$$y(x) \sim \pm\sqrt{\frac{x}{2}} \pm (2x)^{-1/4}\rho \times \cos\left[\frac{2\sqrt{2}}{3}x^{3/2} - \frac{3}{2}\rho^2 \ln x + \theta\right] \tag{24}$$

Both solutions are oscillatory, with an amplitude that dies off very slowly (with $x^{-1/4}$). The positive asymptote has two parabolic branches, as expected.

[75] Because the Painlevé-II equation has no singularities, the two asymptotic solutions are related to each other via the following connection formulas [*Its and Kapaev*, 1988]:

$$\rho^2 = \frac{1}{\pi}\ln\frac{1+|p|^2}{2|\mathrm{Im}p|} \tag{25}$$

$$\theta = -\frac{\pi}{4} + \frac{7}{2}\rho^2 \ln 2 - \arg\Gamma\left(i\rho^2\right) - \arg\left(1+p^2\right) \tag{26}$$

where

$$p = \left(e^{\pi\alpha^2} - 1\right)^{1/2} \times \exp i\left\{\frac{3}{2}\alpha^2 \ln 2 - \frac{\pi}{4} - \arg\Gamma(i\alpha^2/2) - \varphi\right\} \tag{27}$$

When $\mathrm{Im}\, p < 0$, the solution takes the positive branch, i.e., the upper sign is taken in equation (24). By means of these connection formulas, it is possible to relate the initial value of the second invariant to the post-crossing value.

[76] The exact solution converges to the asymptotic solutions (23) and (24) rather quickly, especially for small values of α and ρ. Except for several bounces around the bifurcation line, the asymptotic expressions are a very good approximation to the real motion.

[77] In the transformed coordinates (x,y), the action is defined as $\oint y'dy$ (over one cycle). Consider an initial "time" $-x_0$ with $x_0 > 0$ and sufficiently large. Evaluating the derivative $y'(x)$ from equation (23) and ignoring the $\mathcal{O}(x_0^{-5/4})$ and higher terms in the derivative, we see that the phase-space profile consists of ellipses:

$$\left(\frac{y(-x_0)}{x_0^{-1/4}}\right)^2 + \left(\frac{y'(-x_0)}{x_0^{1/4}}\right)^2 = \alpha^2 \tag{28}$$

and therefore the action J^- in the negative asymptote, which is the area inside that ellipse, is equal to $\pi\alpha^2$.

[78] For the positive asymptote we proceed in a similar manner. At sufficiently large "time" $x_1 > 0$, after ignoring terms of order $x_1^{-5/4}$, the phase-space curve is again found to be an ellipse:

$$\left(\frac{y(x_1)-\sqrt{x_1/2}}{(2x_1)^{-1/4}}\right)^2+\left(\frac{y'(x_1)-1/\sqrt{8x_1}}{(2x_1)^{1/4}}\right)^2=\rho^2 \tag{29}$$

(only one of the branches is given; the other branch has the same area). Then, the action J^+ in the positive asymptote (several bounces after the crossing) is equal to $\pi\rho^2$. So we see that the amplitude connection formula (25) gives the relation between the initial (single branch) and final (double branch) actions. After substitution of p into equation (25), some algebraic manipulation gives the postcrossing amplitude ρ^2 in terms of the initial amplitude α^2 and phase φ:

$$\rho^2=\alpha^2-\frac{1}{2\pi}\ln\left(e^{\pi\alpha^2}-1\right)-\frac{1}{\pi}\ln\left|2\sin\left[\frac{3}{2}\alpha^2\ln 2-\frac{\pi}{4}-\arg\Gamma\left(\frac{i\alpha^2}{2}\right)-\varphi\right]\right| \tag{30}$$

We skip the phase formula $\theta(\alpha^2, \varphi)$, which can be obtained similarly.

[79] For the inverse process (crossing the conjugate bifurcation line, to a single branch), we need to express α^2 in terms of given ρ^2 and θ. To that end, we invert the connection formulas (25) and (26). After some straightforward algebra, we can express p as a function of ρ^2 and θ as follows:

$$p(\rho,\theta)=ie^{\pi\rho^2}+\left(e^{2\pi\rho^2}-1\right)^{1/2}\exp i\psi \tag{31}$$

where

$$\psi(\rho,\theta)\equiv\left[\theta-\frac{7\ln 2}{2}\rho^2+\frac{3\pi}{4}+\arg\Gamma\left(i\rho^2\right)\right] \tag{32}$$

[80] The variable ψ is introduced as a shorthand to the phase of p. From the definition in equation (27) of p, it follows that:

$$\alpha^2=\frac{1}{\pi}\ln\left(1+|p|^2\right) \tag{33}$$

Direct substitution of $p(\rho, \theta)$ and algebraic manipulation shows that:

$$\alpha^2=2\rho^2+\frac{1}{\pi}\ln\left(2+2\sqrt{1-e^{-2\pi\rho^2}}\sin\psi(\rho,\theta)\right) \tag{34}$$

5.3. Change of the Second Invariant With Small Initial Values

[81] The inverse transformation $x\rightarrow a^{1/3}t$, $y\rightarrow\sqrt{\frac{b}{2}}\,a^{-1/3}s$ will convert the results of the previous subsection back into the bounce problem. We have already established that the action of the single branch solution is $J^- = \pi\alpha^2$, and that of the double branch is $J^+ = \pi\rho^2$, and the relation between them can be determined with the connection formulas (30) and (34). To see how the action in (x,y) space is related to the second invariant, we apply the inverse transformation:

$$J\equiv\oint\frac{\mathrm{d}y}{\mathrm{d}x}\mathrm{d}x=\frac{b}{2a}\oint\frac{\mathrm{d}s}{\mathrm{d}t}\mathrm{d}s \tag{35}$$

$$=\frac{b}{a}\upsilon I \tag{36}$$

[82] Consider a particle that is initialized on the night side with initial second invariant I_0, which then undergoes DSB. Then from equations (30) and (36) above, the next value I_1 of the second invariant can be determined.

$$I_1=I_0-\frac{\zeta}{2}\ln\left(e^{I_0/\zeta}-1\right)-\zeta\ln|2\sin\Phi| \tag{37}$$

where ζ is a scale factor that depends on the geometry of the bifurcation line as well as the particle speed:

$$\zeta\equiv\frac{a}{bv}=\frac{6\mathbf{v}_\mathrm{G}\cdot\nabla_\perp\left|B^{(2)}\right|}{vB^{(4)}} \tag{38}$$

Note that the derivatives $B^{(2)}$ and $B^{(4)}$ are taken along the field line, and evaluated at the equator.

[83] The phase factor Φ is given as:

$$\Phi\equiv\frac{3\ln 2}{2\pi}\frac{I_0}{\zeta}-\frac{\pi}{4}-\arg\left[\Gamma\left(\frac{i}{2\pi}\frac{I_0}{\zeta}\right)\right]-\varphi \tag{39}$$

[84] The result in equation (37) displays a formal resemblance to the nonequatorial result in equation (14), except for the middle term $\frac{\zeta}{2}\ln\left(e^{I_0/\zeta}-1\right)$. In the limit $I_0\gg\zeta$, this middle term reduces to $I_0/2$, thus restoring the form of equation (14).

[85] Conversely, we can show that in the limit of small bounce motion, the factor of the logarithmic term in equation (14) is approximated by ζ. To see this, we write Υ as:

$$\Upsilon=2\int_0^{s_\mathrm{m}}\sqrt{\frac{|B^{(2)}|s^2}{2B_\mathrm{m}}-\frac{B^{(4)}s^4}{24B_\mathrm{m}}}\mathrm{d}s \tag{40}$$

$$=\frac{4\sqrt{2}\left|B^{(2)}\right|^{3/2}}{B_\mathrm{m}B^{(4)}} \tag{41}$$

which is valid for small bounce amplitudes. With the assumption that the fourth derivative $B^{(4)}$ does not change significantly along the drift path up to the bifurcation, we write:

$$\nabla\Upsilon\approx\frac{6\sqrt{2}\left|B^{(2)}\right|^{1/2}}{B_\mathrm{m}B^{(4)}}\nabla\left|B^{(2)}\right| \tag{42}$$

Solving for $\nabla|B^{(2)}|$ and substituting into equation (38) gives

$$\zeta\approx\frac{B_\mathrm{m}^{1/2}}{\sqrt{2}\upsilon|B^{(2)}|^{1/2}}\mathbf{v}_\mathrm{G}\cdot\nabla\Upsilon \tag{43}$$

which is exactly the same as the coefficient of the logarithmic term in equation (14). However, this approximation does not give the middle term of equation (37), which was derived for small initial second invariant. Equations (14) and (37) are complementary in the sense that they are compatible in limiting cases but neither one is a special case of the other. In practice, there is an overlap interval where I is not very small but equation (37) remains applicable.

[86] A uniform ensemble of particles that share the same drift shell have the same value for I_0, and are uniformly distributed in Φ. If I_0 is comparable to ζ, the ensemble average of $\Delta I \equiv 2I_1 - I_0$ will be nonzero because of the middle term: the second invariant of the whole ensemble will shift up by a constant factor as observed in Figure 6. Furthermore, as $I_0/\zeta \to 0$, this constant shift can be arbitrarily large (but increasing only logarithmically).

[87] *Chirikov and Vecheslavov* [2000], who observe a similar effect in another system, use the term "ballistic regime" for very small action values where the whole population experiences a large action jump. In contrast, large values of initial action are in the "diffusive regime" because an ensemble of particles is scattered onto a small range of action values, with an average change of zero. The case of nonequatorial particles, analyzed in the preceding section, corresponds to the diffusive regime.

[88] Now consider a particle that is already in the bifurcation region and happens to have a very small second invariant I_1. When the particle drifts across the conjugate bifurcation line, it acquires the nightside second invariant value I_2. The value of I_2 can be determined with the connection formulas (34) and (36):

$$I_2 = 2I_1 + \zeta \ln\left(2 + 2\sqrt{1 - e^{-2I_1/\zeta}} \sin\Psi\right) \tag{44}$$

with

$$\Psi \equiv \theta - \frac{7\ln 2}{2\pi}\frac{I_1}{\zeta} + \frac{3\pi}{4} + \arg\left[\Gamma\left(\frac{i}{\pi}\frac{I_1}{\zeta}\right)\right] \tag{45}$$

It should be noted that ζ does not have the same value as in equation (37), but needs to be reevaluated at the new bifurcation line. Again, in the limit $I_1 \gg \zeta$, the expression has the same form as the nonequatorial solution (15) (to see this, the argument of the logarithm needs to be manipulated using trigonometric identities). Note that in the opposite limit $I_1 \ll \zeta$, the jump in the second invariant is finite: $\Delta I \equiv I_2 - 2I_1 = \zeta \ln 2$.

5.4. Numerical Study

[89] The analysis of the previous subsection shows that ζ is the key parameter for the second-invariant jump. Substituting for the gradient drift velocity, equation (38) can be written as:

$$\zeta = \rho_m 3\,\mathrm{sgn}(q)\frac{\left(\hat{b}\times\nabla_\perp B\right)\cdot\nabla_\perp\left|B^{(2)}\right|}{B_m B^{(4)}} \tag{46}$$

The factors $B^{(2)}$ and $B^{(4)}$ are the second and fourth derivatives of field strength along the field line, respectively. We can rewrite this as $\zeta \equiv \rho_m F$, introducing a new parameter F that depends only on the geometric properties of the magnetic field and the drift shell. The expression should be evaluated at the bifurcation point, which is the intersection of the contour $B = B_m$ (the drift path) and the boundary of the bifurcation region.

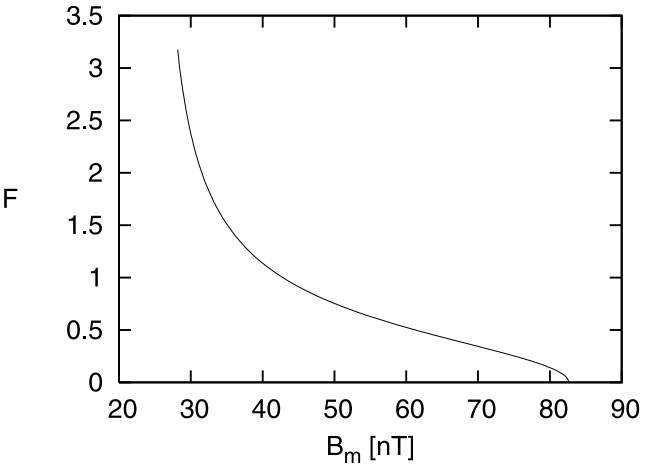

Figure 11. The ballistic parameter F versus the mirror field values, for the double-dipole field. Small B_m corresponds to drift shells at large distances from the Earth and thus bifurcate farthest from local noon.

[90] To compare this theoretical result with the simulations presented in section 3, we evaluate F in the case of a double-dipole field whose details are described earlier. Every point along the edge of the bifurcation region corresponds to a different value of the mirror field B_m of the drift shell, so we can treat F as a function of B_m. Figure 11 shows a plot of F versus B_m for the double-dipole field. We see that F varies between 0 and 3, thus the parameter ζ varies between 0 and $3\rho_m$.

[91] The electron-ensemble simulations of Figure 6 are both produced using a mirror field value of 41.88 nT and an initial second invariant $I_0 = 1.2\times10^{-3}\ R_e$. From Figure 11, we read that this value predicts an $F \approx 1.04$. The 175-keV electrons have a mirror gyroradius of $5.72\times10^{-3}\ R_e$, thus $\zeta = \rho_m F = 5.95\times10^{-3}\ R_e$. With these values in place, equation (37) predicts

$$2I_1 - I_0 = (10.11 - 11.9\ln|2\sin\phi|)\times10^{-3}R_e \tag{47}$$

which is in agreement with the numerical fit to the data in Figure 6, except for a constant shift in the phase of all particles.

[92] The 413-keV electrons have a mirror gyroradius of $9.65\times10^{-3}\ R_e$, thus $\zeta = 10.04\times10^{-3}\ R_e$. Therefore for this data set, equation (37) predicts

$$2I_1 - I_0 = (21.9 - 20.1\ln|2\sin\phi|)\times10^{-3}R_e \tag{48}$$

which again agrees well with the synthetic data from simulations. The theory presented in this section successfully explains the ballistic jump in the second invariant.

[93] One can easily apply the method to different magnetospheric models, first by determining the edge of the bifurcation region (the set of points at the equatorial plane

satisfying $dB/ds = 0$), and then by evaluating F at every point in this set.

6. Magnetospheric Implications

[94] In this study, we focused on the analysis of single crossings and deferred the analysis of multiple crossings to another article. However, we would like to share two of the important implications of DSB for drift shells that cross the bifurcation region many times.

[95] The first effect is the existence of a diffusive mechanism in a constant magnetosphere. At each bifurcation point, the second invariant makes a jump, which in the long term can be seen as a random walk because the phase information cannot be easily tracked. This corresponds to two radial displacements at each drift cycle.

[96] Researchers are now beginning to combine models of the radiation belts that represent transport in terms of diffusion coefficients with numerical MHD models of large-scale magnetospheric dynamics, which calculate the magnetic field configuration as a function of time. DSB-transport effects could be incorporated approximately in those models in terms of a diffusion coefficient $\langle \Delta I^2 \rangle / 2\Delta t$. A full treatment of this diffusion coefficient will require a statistical treatment, which we defer to a later study. However, the order-of-magnitude of the diffusion coefficient can be estimated as:

$$D_{II} = \frac{\langle \Delta I^2 \rangle}{2\tau_d} \sim 0.411 \frac{\rho_m^2}{\tau_d} \left(G_{dawn}^2 + G_{dusk}^2 \right) \tag{49}$$

where $0.411 = (1/4\pi) \int_0^{2\pi} \ln^2 |2\sin\phi| \, d\phi$, the parameter τ_d is the drift period, and G_{dawn}, G_{dusk} are the G factors at the two bifurcation lines, varying between 0.1 and 10.

[97] We estimate (see the Appendix) that the radial transport due to DSB becomes comparable to magnetic-noise-induced diffusion, as estimated by extrapolating the *Brautigam and Albert* [2000] formula to the near-magnetopause region, for electron energies above 10 MeV, in order of magnitude. Pitch angles are also altered by the process, at a rate that increases rapidly with energy. Of course, this mechanism only operates on particles whose trajectories come within $1-2\ R_e$ of the magnetopause and only for particles with equatorial pitch angles close enough to $\pi/2$ that they undergo drift-shell bifurcation.

[98] The second effect, related to the first, is the emergence of a new type of trapping. Traditionally, energetic particle trajectories in static-magnetic field configurations have been divided into three categories: (1) stably trapped, which refers to drift paths that circle the Earth infinitely many times; (2) quasi-trapped, which refers to particles that bounce between mirror points on closed field lines but cross the magnetopause without completing one complete drift around the Earth; and (3) untrapped, which refers to particles that move only on open or interplanetary field lines. The random walk in the radial coordinate due to DSB implies that a particle with mirror field $B_m < B_{subsolar}$ may drift around the Earth once (or many times) before its second invariant becomes sufficiently large so that it drifts into the magnetopause and presumably escapes. We propose referring to this new class of particles as "metastably trapped".

7. Conclusions

[99] Drift-shell bifurcation is a result of the dayside compression of the magnetosphere. It mainly affects particles that drift close to the magnetopause. The nonadiabatic interruption of the bounce motion causes a permanent change in the second invariant, which is conserved everywhere except around the bifurcation lines.

[100] Simulations and analysis show that particles with high energies and with large equatorial pitch angles ($\alpha_{eq} > 80^\circ$) are strongly affected by the violation of the second invariant. Similarly, shells that bifurcate at the dawnside or duskside edges of the bifurcation region are more affected than those which bifurcate near local noon. When we let a set of particles which have the same energy and occupy the same drift shell, but differ by bounce phase, drift across the bifurcation line, we see that they all acquire different second invariant values. That is, they are scattered onto neighboring drift shells.

[101] We have presented an analysis of the magnitude of the second-invariant change, which can be directly applied to any magnetic field model that is static and possesses north-south symmetry. We identify two parameter regimes: The diffusive regime, where the prebifurcation value of the second invariant is much larger the mirror gyroradius of the particle's motion. Such cases are analyzed with the CET formula. In that regime, the average change of the second invariant in a bounce-phase ensemble is zero, but the root mean square change is not zero. When the ensemble is prepared so that the initial second invariant is of the same order as, or less than, the mirror gyroradius, we see an overall shift in the second invariant in addition to the diffusive term. This is called the ballistic regime, where each particle is catapulted onto a significantly distant drift shell. This case precludes the use of the CET formula, but the Painleve formula is applicable here. These two cases complement each other to provide a complete picture of the DSB effect.

[102] Our results are equally applicable to both ions and electrons, provided that the guiding-center approximation is valid.

[103] Our analysis is based on certain simplifications: constant magnetic field, zero electric field, and north-south symmetry. These assumptions can be relaxed. Even in the presence of electric fields or time-varying magnetic fields, if the conditions are adiabatic, we can assume that I is a valid invariant for a few bounces around the bifurcation line. Then, the formulas in this article can still be used to relate second-invariant values just before and just after bifurcation. We can also relax the symmetry requirement by replacing the references to the equatorial plane with the surface satisfying $dB/ds = 0$. However, the results of separatrix-crossing theory by *Cary et al.* [1986] are more complicated when such symmetry lacks.

[104] When the interplanetary magnetic field has a strong y-component, some of that B_y "leaks" into the magnetosphere, resulting in a magnetospheric configuration where neither north-south nor dawn-dusk symmetry exists. Such an asymmetry may give rise to a different DSB-associated mechanism for violating the second invariant. Suppose an

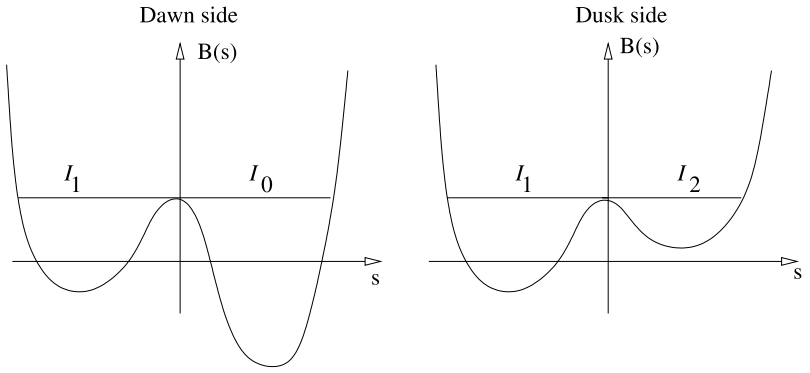

Figure 12. Schematic view of DSB under asymmetric conditions. An electron with initial second invariant $I_0 + I_1$ undergoes bifurcation at the dawn side (left) and leaves the bifurcation region later with a different invariant $I_1 + I_2$. Note that the change in the invariant is of zeroth order, not sensitively depending on the bounce phase or on the energy of the particle.

electron with second invariant $I_0 + I_1$ and mirror field B_m arrives at the dawnside bifurcation point from the dawn side (Figure 12, left diagram) and gets trapped in the Southern Hemisphere with invariant I_1 (we ignore the first-order corrections here), the electron drifts past noon conserving the invariant and arrives at the duskside bifurcation point (Figure 12 diagram). After passing that point, its invariant will be $I_1 + I_2$, which is less than its initial invariant, since $I_0 > I_2$. Conversely, an electron that gets trapped in the Northern Hemisphere at the dawn side will have its second invariant increased.

[105] The change induced by this asymmetry mechanism depends neither on bounce phase (except to determine on which side the particle will be trapped), nor on the energy of the particle. As such, it is of zero order in the gyroradius, while the bounce-phase-dependent change we investigated throughout the present article is a first-order effect. Under general conditions, the asymmetric effect can be as significant as the bounce-phase effect we considered in this article. For particles that undergo DSB with lower energies, it may be the dominant agent for the changes in the second invariant. We leave the detailed analysis of this effect to a later study.

[106] The aim of this paper has been to expose the basic physics involved in the violation of the second invariant upon bifurcation. The work was done partly because we felt it might be useful in future modeling studies of radiation-belt physics. Of course, drift-shell bifurcation does not occur in the heart of the radiation belts, so the work reported here does not directly impact classical radiation-belt-diffusion models. However, knowledge of transport through the DSB region may prove useful in theoretical study of the sources of radiation-belt particles, since the DSB region lies between the radiation belts and two often-mentioned possible source regions: the plasma sheet [e.g., *Baker et al.*, 1998] and the polar cusps [*Sheldon et al.*, 1998]. Furthermore, careful theoretical treatment of the trapping boundary and loss through the magnetopause requires treatment of transport in the DSB region.

Appendix A: Estimates of Radial and Pitch-Angle Diffusion Coefficients

[107] This Appendix presents approximate expressions on how D_{II} given in equation (49) relates to radial and pitch angle diffusion coefficients. Within the assumptions we made in this study, there is no diffusion in energy because the energy is kept constant.

A1. Radial Diffusion

[108] To estimate the radial diffusion that corresponds to D_{II}, consider particles mirroring near the equator, where the magnetic field is a minimum and we approximate $B(s)$ as a Taylor series in s up to second order. This gives

$$I \approx \frac{\pi s_m^2}{2}\sqrt{\frac{B''}{2B_0}} \tag{A1}$$

where s_m is the distance from the equator to the mirror point, B_0 is the equatorial magnetic field, and B'' is the second derivative of B with respect to distance along the field line, evaluated at the equator. In order to estimate the relevant quantities, we will assume that the realistic values will be in the same order of magnitude as the dipolar values. *Walt* [1994] provides expressions for field lines and $B(s)$ under a dipole field. In a dipole, we have:

$$B'' = \frac{9B_0}{L^2R_e^2} \tag{A2}$$

so that

$$s_m^2 = \frac{2L^2R_e^2}{9B_0}(B_m - B_0) \tag{A3}$$

Combining these three equations and using the dipole formula for B_0 gives:

$$I \approx \frac{\pi LR_e}{3\sqrt{2}}\left(\frac{B_mL^3}{B_e} - 1\right) \tag{A4}$$

where B_e is the field strength at the Earth's equator. Differentiating with respect to L, while holding B_m (and thus energy) constant, gives:

$$\left[\frac{\partial I}{\partial L}\right]_{B_m} \approx \frac{\pi R_e}{\sqrt{2}}\left(\frac{4}{3}\frac{B_m}{B_e}L^3 - \frac{1}{3}\right) \tag{A5}$$

Here $B_m L^3 / B_e = B_m / B_0 \approx 1$ because we assumed that the particle is mirroring near the equatorial plane. Then, the right-hand side reduces to $\pi R_e/\sqrt{2}$ and we have

$$\Delta L \approx \frac{\sqrt{2}}{\pi R_e} \Delta I \tag{A6}$$

which, in turn, gives the following approximate relation between diffusion coefficients:

$$D_{LL} \approx \frac{2}{\pi^2 R_e^2} D_{II} \tag{A7}$$

To get a numerical estimate, we again assume a dipolar magnetic field and consider ultrarelativistic electrons, obtaining:

$$\left(\frac{\rho_m^2}{\tau_d}\right)_{UR} = \left(\frac{\gamma m_e c}{qB}\right)^2 \frac{3\gamma m_e c^2}{4\pi q B r^2} \tag{A8}$$

Here we assume an equatorial trajectory, so τ_d is the gradient drift period and r is the radius of the drift path. This equation can be converted to a numerical formula as follows:

$$\left(\frac{\rho_m^2}{\tau_d}\right)_{UR} \approx \left(0.047 \frac{R_e^2}{\text{day}}\right) W_{MeV}^3 \left(\frac{L}{10}\right)^7 \tag{A9}$$

where $W_{MeV} = \gamma m_e c^2$ in units of MeV. Substituting equation (A9) in equation (49) gives the following estimated diffusion coefficient for ultra-relativistic electrons:

$$D_{LL}^{DSB,UR} \sim (0.0039 \text{ day}^{-1}) W_{MeV}^3 \left(\frac{L}{10}\right)^7 \left(G_{dawn}^2 + G_{dusk}^2\right) \tag{A10}$$

Brautigam and Albert [2000] give the following empirical formula for magnetic diffusion of electrons:

$$\left(D_{LL}^M\right)_{B\&A} = 10^{0.675+0.506K_p} \left(\frac{L}{10}\right)^{10} \tag{A11}$$

Of course, the Brautigam-Albert formula was not really intended for use near the magnetopause, but if we nonetheless use it at $L \approx 10$, we conclude that drift-shell bifurcation effects become competitive with magnetic-fluctuation-induced radial diffusion for $W > 10$ MeV, for a typical DSB electron ($G \sim 1$). Furthermore, it is clear from Figures 8, 9, and 10 that electrons with relatively small B_m may acquire $G \sim 10$ and thus experience significantly stronger diffusion. If we apply equation (49) to nonrelativistic ions, we obtain a much higher estimate for the diffusion rate:

$$D_{LL}^{DSB,NR} \sim \left(14.6 \text{ day}^{-1}\right) A K_{MeV}^2 \left(\frac{L}{10}\right)^7 \left(G_{dawn}^2 + G_{dusk}^2\right) \tag{A12}$$

because the ions have much larger gyroradii. Here A is the atomic weight of the ion, and K_{MeV} is the kinetic energy, in units of million electron volts.

[109] Formulas (A9) and (A12) can provide only very rough estimates and should be applied with caution. It should, of course, be borne in mind that drift-shell bifurcation only occurs for particles whose drift orbits take them within 1–2 R_e of the magnetopause, so it does not transport particles through the inner magnetosphere. Also, a particle that drifts into the bifurcation region with extremely small I (of the order of the gyroradius) typically has its I value increased significantly at the first bifurcation point, which reduces the value of G for later encounters with bifurcation points. To get a better idea of the overall effectiveness of DSB-associated transport, it will be necessary to perform test-particle calculations of large numbers of particles in realistic magnetic fields under various conditions.

A2. Pitch Angle Diffusion

[110] Conservation of the first invariant implies that

$$\frac{\sin^2 \alpha}{B} = \frac{1}{B_m} \tag{A13}$$

Let $\psi \equiv \pi / 2 - \alpha$ and assume that $|\psi| \ll 1$, which typically holds for DSB trajectories. Replacing $\sin^2\alpha$ by $1 - \psi^2$ gives:

$$\psi_0^2 \approx \frac{B'' s_m^2}{2B_0} \tag{A14}$$

where the subscript "0" indicates an equatorial value. Substituting equation (A14) into equation (A1) gives

$$\psi_0^2 \approx \frac{2}{\pi} \left(\frac{B''}{2B_0}\right)^{1/2} I \tag{A15}$$

Assuming that the change ΔI is small compared to I, we get

$$(\Delta\psi_0)^2 \approx \frac{1}{2\pi} \left(\frac{B''}{2B_0}\right)^{1/2} \frac{(\Delta I)^2}{I} \tag{A16}$$

So that the pitch angle scattering coefficient is related to D_{II} by

$$D_{\psi_0\psi_0} = D_{\alpha_0\alpha_0} = \frac{(\Delta\psi_0)^2}{2\tau_d} \tag{A17}$$

$$= \frac{1}{2\pi} \left(\frac{B''}{2B_0}\right)^{1/2} \frac{D_{II}}{I} \tag{A18}$$

Finally, using equations (A2) and (A15) gives the relation between D_{II} and the pitch angle diffusion coefficient:

$$D_{\alpha_0\alpha_0} \sim \frac{9}{2\pi^2 L^2 R_e^2} \frac{D_{II}}{(\pi/2 - \alpha_0)^2} \tag{A19}$$

$$= 0.187 \frac{\rho_m^2 (G_{dawn}^2 + G_{dusk}^2)}{L^2 R_e^2 (\pi/2 - \alpha_0)^2 \tau_d} \tag{A20}$$

where we used equation (49) to derive the last relationship.

[111] Equation (A19), which indicates very large values for the diffusion coefficient for α_0 near $\pi/2$, was based on the perturbation analysis presented in section 4. It is invalid when the change in pitch angle is greater than or comparable to $\pi/2 - \alpha_0$. Define a critical value of $\psi_0 = \pi/2 - \alpha_0$ such that $D_{\alpha_0\alpha_0} \sim \psi_{0,\mathrm{crit}}^2 / 2\tau_\mathrm{d}$, which implies that:

$$\psi_{0,\mathrm{crit}} = \left[2 \cdot 0.187 \frac{\rho_\mathrm{m}^2}{L^2 R_\mathrm{e}^2}\left(G_\mathrm{dawn}^2 + G_\mathrm{dusk}^2\right)\right]^{1/4} \tag{A21}$$

$$\sim 0.032\, W_\mathrm{MeV}^{1/2}\left(\frac{L}{10}\right)\left(G_\mathrm{dawn}^2 + G_\mathrm{dusk}^2\right)^{1/4} \tag{A22}$$

where the last equality applies to ultra-relativistic electrons only. Then equation (A19) can be rewritten as:

$$D_{\alpha 0\alpha 0} \sim \sqrt{\frac{0.187}{2}}\frac{\rho_\mathrm{m}\sqrt{G_\mathrm{dawn}^2 + G_\mathrm{dusk}^2}}{LR_\mathrm{e}\tau_\mathrm{d}\left(\psi_0/\psi_{0,\mathrm{crit}}\right)^2} \tag{A23}$$

$$\sim (0.085\ \mathrm{day}^{-1}) W_\mathrm{MeV}^2\left(\frac{L}{10}\right)^3 \times \frac{\sqrt{G_\mathrm{dawn}^2 + G_\mathrm{dusk}^2}}{\left(\psi_0/\psi_{0,\mathrm{crit}}\right)^2} \tag{A24}$$

Equation (A23) is valid for ψ_0 greater than about $\psi_{0,\mathrm{crit}}$. The second equality [equation (A24)] applies to ultrarelativistic electrons only.

[112] The authors are not aware of detailed treatments of other pitch angle scattering mechanisms for relativistic electrons near the magnetopause, but much work has been done on pitch angle scattering rates for the heart of the outer radiation belt at $L \sim 4$–5, where whistler mode chorus waves are believed to play an important role. Figure 1 of *Glauert and Horne* [2005] shows $D_{\alpha_0\alpha_0}$ values of 9–130 day^{-1} for 1 MeV electrons with $\alpha \approx \pi/2$ and $L = 4.5$, while Figure 1 of *Summers* [2005] shows values of 260 day^{-1} and 9 day^{-1} for 1 MeV and 3 MeV, respectively. Thus the pitch angle scattering associated with drift-shell bifurcation, for electrons with a few million electron volts of energy, seems to be at least two orders of magnitude slower than the rate estimated for whistler mode chorus waves in the heart of the outer radiation belts.

[113] **Acknowledgments.** The authors are grateful to Seth Orloff for pointing out the violation of adiabaticity in simulated particle orbits, and to Anthony Chan, Stephen Naehr, and Mike Schulz for many valuable discussions. This work was supported by the NASA grant NAG5-9077, NSF Space Weather grant ATM-0208350, and by NASA Sun-Earth-Connections Theory grants NAG5-11881 and NNG05GH93G.

[114] Amitava Bhattacharjee thanks Jay Albert and Mary K. Hudson for their assistance in evaluating this paper.

References

Albert, J. M. (1993), Cyclotron resonance in an inhomogeneous magnetic field, *Phys. Fluids*, *B*(5), 2744–2750.

Antonova, A. E., Yu. I. Gubar, and A. P. Kropotkin (2003), Effects in the radiation belts driven by the second adiabatic invariant violation in the presence of high-latitude field minimums in the dayside cusps, *Geomagn. Aeron.*, *43*(1), 1–6 (English translation).

Baker, D. N., X. Li, J. B. Blake, and S. Kanekal (1998), Strong electron acceleration in the Earth's magnetosphere, *Adv. Space Res.*, *21*(4), 609–613.

Bazzani, A. (1999), Adiabatic invariance for pendulum-like systems, *Il Nuovo Cimento*, *112 A*(5), 437–446.

Brautigam, D. H., and J. M. Albert (2000), Radial diffusion analysis of outer radiation belt electrons during the October 9, 1990, magnetic storm, *J. Geophys. Res.*, *105*(A1), 291–309.

Büchner, J., and L. M. Zelenyi (1989), Regular and chaotic charged particle motion in magnetotaillike field reversals: 1. Basic theory of trapped motion, *J. Geophys. Res.*, *94*(A9), 11,821–11,842.

Bulanov, S. V., and N. M. Naumova (1996), Change of adiabatic invariant near the separatrix, *Phys. Scr.*, *T63*, 190–196.

Cary, J. R., and R. T. Skodje (1989), Phase change between separatrix crossings, *Physica D*, *36*, 287–316.

Cary, J. R., D. F. Escande, and J. L. Tennyson (1986), Adiabatic-invariant change due to separatrix crossing, *Phys. Rev. A*, *34*(5), 256–275.

Chapman, S., and J. Bartels (1940). Geomagnetism, Chapter XXV, Oxford Univ. Press, New York.

Chirikov, B. V., and V. V. Vecheslavov (2000), Adiabatic invariance and separatrix: Single separatrix crossing, *J. Exp. Theor. Phys.*, *90*(3), 562–569.

Clarkson, P. A. (2003), Painlevé equations—Nonlinear special functions, *J. Comput. Appl. Math.*, *153*, 127–140.

Delcourt, D. C., and J.-A. Sauvaud (1998), Recirculation of plasma sheet particles into the high-latitude boundary layer, *J. Geophys. Res.*, *103*(A11), 26,521–26,532.

Delcourt, D. C., and J.-A. Sauvaud (1999), Populating of the cusp and boundary layers by energetic (hundreds of keV) equatorial particles, *J. Geophys. Res.*, *104*(A10), 22,635–22,648.

Glauert, S. A., and R. B. Horne (2005), Calculation of pitch angle and energy diffusion coefficients with the PADIE code, *J. Geophys. Res.*, *110*, A04206, doi:10.1029/2004JA010851.

Henrard, J. (1993), The adiabatic invariant in classical mechanics, in Dynamics Reported (New Series): Expositions in dynamical systems, edited by C.K. R. T. Jones, U. Kirchgraber and H.-O. Walther, pp. 117–235, Springer, New York.

Its, A. R., and A. A. Kapaev (1988), The method of isomonodromy deformations and connection formulas for the second Painlevé transcendent, *Math. USSR Izvestiya*, *31*(1), 193–207 (English translation).

Mead, G. D. (1964), Deformation of the geomagnetic field by the solar wind, *J. Geophys. Res.*, *69*(7), 1181–1195.

Northrop, T. G. (1963), The adiabatic motion of charged particles, Wiley-Interscience, Hoboken, N. J.

Northrop, T. G., and E. Teller (1960), Stability of adiabatic motion of charged particles in the Earth's field, *Phys. Rev.*, *117*(1), 215–225.

Orloff, S. (1998), A computational investigation of solar energetic particle trajectories in model magnetospheres, Ph.D. thesis, Rice University, Houston, Texas, June 1998.

Roederer, J. G. (1970), Dynamics of Geomagnetically Trapped Radiation, Springer, New York.

Shabansky, V. P. (1971), Some processes in the magnetosphere, *Space Sci. Rev.*, *12*(3), 299–418.

Shabanskiy, V. P., and A. Ye. Antonova (1968), Topology of the drift shells of particles in the magnetosphere, *Geomagn. Aeron.*, *8*, 799–802 (English translation).

Sheldon, R. B., H. E. Spence, J. D. Sullivan, T. A. Fritz, and J. Chen (1998), The discovery of trapped energetic electrons in the outer cusp, *Geophys. Res. Lett.*, *25*(11), 1825–1828.

Summers, D. (2005), Quasi-linear diffusion coefficients for field-aligned electromagnetic waves with applications to the magnetosphere, *J. Geophys. Res.*, *110*, A08213, doi:10.1029/2005JA011159.

Tsyganenko, N. A. (1989), A magnetospheric field model with a warped tail current sheet, *Planet. Space Sci.*, *37*, 5–20.

Vainshtein, D. L., L. M. Zelenyi, A. I. Neishtadt, and B. V. Savenkov (1999), Jumps in an adiabatic invariant with small initial values, *Plasma Phys. Rep.*, *25*(4), 299–303 (English translation).

Walt, M. (1994), Introduction to Geomagnetically Trapped Radiation. Cambridge Univ. Press, New York.

Young, S. L., R. E. Denton, B. J. Anderson, and M. K. Hudson (2002), Empirical model for μ-scattering caused by field line curvature in a realistic magnetosphere, *J. Geophys. Res.*, *107*(A6), 1069, doi:10.1029/2000JA000294.

M. K. Öztürk, Department of Information Technologies, Işık University, Kumbaba Mevkii, İstanbul, Turkey. (mkozturk@isikun.edu.tr)

R. A. Wolf, Department of Physics and Astronomy, Rice University, MS 108, 6100 Main St., Houston, TX 77005, USA. (rawolf@rice.edu)